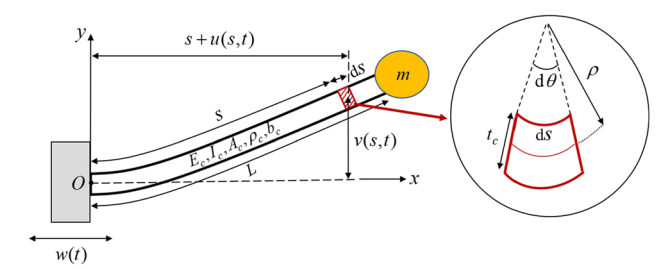
Regular Article

Hany Samih Bauomy*

Advanced vibrant controller results of an energetic framework structure

https://doi.org/10.1515/eng-2024-0055 received February 21, 2024; accepted June 06, 2024

Abstract: This research shows the influence of a new active controller technique on a parametrically energized cantilever beam (PECB) with a tip mass model. This article remains primarily concerned with regulating the system's response using a novel control mechanism. This study describes a novel control mechanism called the nonlinear proportional-derivative cubic velocity feedback controller (NPDCVFC). The motivation of this article is to design a novel control algorithm in order to mitigate the nonlinear vibrations of a parametrically energized cantilever beam with a tip mass model. The proposed controller NPDCVFC incorporates nonlinearly second- and first-order filters into the system. The system is governed by one nonlinear differential equation having both quadratic and cubic nonlinearities within the parametric force. The controller's efficiency in reducing framework vibrations, managing nonlinear bifurcations, and calming unstable motion is evaluated using numerical simulations of instantaneous vibrations. The perturbation technique is beneficial for solving the current model under the proposed worst resonance case ($\hat{\Omega}_p = 2\hat{\omega}_0$). In order to choose the optimal controller, we have also added three more controller approaches to the configuration. Integral resonant control, positive position feedback, and nonlinear integral positive position feedback are the three controller approaches that are applied to the structure under consideration. We determine that the NPDCVFC as a new controller is the most effective for lowering the high vibration amplitudes. Over the investigated model, all numerical results were performed using the MATLAB 18.0 programmer software. The stability analysis and the effects of various elements on the controlled structure have been investigated. A comparison with recently published works of a comparable model has also been prepared.



Graphical abstract

Experiment capacities for a PECB with a tip mass are obtainable to validate the results, and they demonstrate good agreement with analytical and numerical results.

Keywords: parametrically excited, cantilever beam, perturbation, stability, IRC, PPF, NIPPF and NPDCVF controllers

1 Introduction

Applying different types of stimulation to dynamic systems is a widespread activity. Direct excitation, sometimes known as forced excitement, is a common type of stimulation. The system itself, damping, and the amplitude of the excitation all have an impact on the vibration amplitudes of a framework under direct excitation. Huge responses can be obtained in directly excited systems when one of the main frequencies of the model is close to the excitation frequency or when there are significant nonlinearities. Damping or the nonlinearity itself can then limit these massive vibration amplitudes. Be that as it may, on the grounds that the excitation looks like time-fluctuating coefficients in the situation of movement, parametrically animated frameworks show aversion to phenomenally huge vibration amplitudes. The interaction of the parametric excitation and system properties, including inherent frequencies, primarily determines the stability of structural systems. In a frequency region near the fundamental parametric resonance, a tiny excitation amplitude can cause a significant response in the system. Large vibrations that follow could damage the system's components and cause significant dynamic instability before the system collapses. Wind, traffic, and earthquakes are the usual causes of

^{*} Corresponding author: Hany Samih Bauomy, Department of Mathematics, College of Science and Humanities in Alkharj, Prince Sattam Bin Abdulaziz University, Alkharj, 11942, Saudi Arabia; Department of Mathematics, Faculty of Science, Zagazig University, Zagazig, 44519, Egypt, e-mail: hany_samih@yahoo.com

parametric excitation for cable-stayed bridges [1]. Ignoring a substantial correlation between parametric excitation and bridge vibration could have lethal consequences [2–5]. Occasionally, the roll motion of a ship can cause amplitudes that are dangerously high. At the point when the wave level outperforms a specific limit and the wave excitation recurrence is generally two times that of the boat's regular recurrence, the biggest amplitudes are conceivable. The ship may capsize as a result of this parametric roll or abrupt change in vibrational amplitude [6].

Parametric excitation is utilized in a variety of applications, such as vibration suppression, signal identification, response amplification, and vibration energy harvesting. Vibration energy harvesters are devices that transform mechanical energy from environmental vibrations into useful electricity. It has been shown that vibration energy collecting, when done properly, can offer a consistent and efficient energy source for everyday electronic device operation [7]. In vibration energy harvesting, the most commonly employed mechanical to electrical transduction mechanisms include electromagnetic [8], electrostatic [9], piezoelectric [10], and magnetostrictive transduction processes. Parametric amplification, the process of introducing parametric excitation to a directly excited system, makes parametric excitation useful for response amplification [11]. Parametric stimulation has also been shown to be an efficient strategy for vibration reduction. The decrease of the vibrational amplitudes of the main (hosting) system is a critical building component of the parametric vibration suppression technique. The pendulum is the most commonly used structure for suppressing parametric vibration [12].

The huge vibrational amplitudes obtained at principal parametric resonance, on the other hand, have been extensively employed for sensing purposes [13]. The important parametric reverberation is actuated at two times the framework's normal recurrence on the off chance that how much the parametric excitation is adequately enormous to beat energy dissemination in the framework. At long last, the nonlinearities of the framework hose vibrations. The powerful behavior of parametrically energized frameworks has been extensively investigated in a range of applications using parametrically invigorated cantilever radiates [14–20]. Methods of perturbation, such as the method of multiple scales (MMS) [21–26] and averaging approaches [27,28], have frequently been used to investigate the energetic performance of parametrically simulated models. These strategies have been demonstrated to be effective at predicting how such systems will react, particularly in the frequency region near the major parametric resonance [29]. Conventional MMS has been demonstrated to accurately forecast response only under basic parameters of modest system

characteristics, moderate excitations, and confined frequency ranges around the central parametric resonance [15,29–36]. Furthermore, a variety of control mechanism solutions have been explored and demonstrated to lessen the harmful vibrations caused by various nonlinear systems [37-45]. A linear proportional-derivative (PD) controller is implemented to eliminate the nonlinear behaviors and to reduce the lateral oscillations of an asymmetric horizontally supported nonlinear rotor system. The proposed controller is joined to the rotor system through an electromagnetic actuator with four poles. One pair of poles manages system vibrations horizontally, while the other pair handles vertical oscillations, as mentioned in Saeed et al. [46]. Recently, research studies [47,48] presented an eightpole actuator as an alternative to the four-pole actuator for reducing nonlinear vibrations in a Jeffcott system. In their initial research [47], the authors utilized a PD control algorithm with the eight-pole actuator to dampen unwanted vibrations in a nonlinear Jeffcott model suspended vertically. In their later study [48], they employed a proportional integral resonant controller (PIRC) to reduce the nonlinear oscillations in the model analyzed by Saeed et al. [47]. The analysis showed that combining the PIRC control with the eight-pole actuator stabilizes the unstable motion seen with the PD controller. The performance of the positive position feedback (PPF) controller is improved by suppressing its two peaks to acceptable levels, where that could be done by coupling additional nonlinear saturation controllers to the rotating compressor blade system to impose a V-curve at each one of the peaks. Using multiple time-scale method, the approximate solutions were derived, and a stability analysis was achieved in Kandil and Eissa [49]. Also, a macro fiber composite (MFC) system is applied an active control algorithm to mitigate the unwanted vibrations of a rotating blade via MFC sensors and actuators by applying the PPF algorithm [50]. Formerly, a horizontally supported car's motion has been modeled and controlled under the effect of a nonlinear spring, a damper, and a harmonic excitation external force. The car's oscillations were controlled via an integral resonant controller, which was built on a linear variable differential transformer and a servo-controlled linear actuator [51].

This article aims to examine a novel active controller approach for the structure model offered within parametric excitation in the worst-case scenario, which serves as the primary parametric resonance situation ($\hat{\Omega}_p = 2\hat{\omega}_0$) using a perturbation technique and numerical methods. The motivation of this article is to design a novel control algorithm in order to mitigate the nonlinear vibrations of a parametrically energized cantilever beam using a tip mass model. The proposed controller, nonlinear proportional-derivative cubic velocity feedback controller (NPDCVFC), incorporates nonlinear second- and first-order filters into the system. The system

is governed by one nonlinear differential equation having both quadratic and cubic nonlinearities within the parametric force. The controller's efficiency in reducing framework vibrations, managing nonlinear bifurcations, and calming unstable motion is evaluated using numerical simulations of instantaneous vibrations. The requirement for another dynamic regulator approach for this model is to lessen as many hazardous and dangerous vibrations caused by the structure as possible. To avoid these vibrations, the author tried other regulators such as NPD, PPF, and IRC, but found that the NPD was inadequate. Thus, he increased the nonlinear terms in NPD by connecting them through the NCVF regulator, which reduces vibrations more than other regulators. With the help of a corresponding subsidiary regulator and negative cubic speed criticism, the new dynamic control has shown an expansion in nonlinear boundaries and a more noteworthy number of ends of the related system's perilous vibrations. As a new nonlinear control method, NPDCVFC, the explored controller uses NPD plus NCVFC. A numerical comparison is made with various nonlinear controllers that have an impact on the system. The key finding from the numerical result shows that the new controller, NPDCVFC, has the most influence in lowering and getting rid of the high vibrations on the model. MATLAB 18.0 software was used to compute the stability study and the effects of various framework parameters both mathematically and numerically. There has also been a comparison with other recent works on the same concept.

2 Description of the model

Figure 1 describes a cantilever beam with a tip mass m under parametric excitation, where L marks the length of the cantilever, w(t) is the displacement of the clamped end giving parametric excitation, and u(s, t) v(s, t) are the cantilever's axial and transverse deflections, respectively. As illustrated in Aghamohammadi et al. [16], s is the coordinate along the middle plane of the cantilever representing the arc length, ρ_c is the density of the cantilever, b_c signifies the width, t_c is the thickness, A_c is the crosssectional area, E_c designates the elastic modulus, I_c is the area moment of inertia, ho is the radius of curvature, and hetais the angle of rotation. The tip mass m is defined as a point mass added at the cantilever tip (s = L). It is presumed that its moment of inertia is negligible. It is believed that the beam is uniform. Furthermore, the cantilever beam is treated as an Euler-Bernoulli beam, with its thickness assumed to be minimal in relation to its length. Shear deformation and rotating inertia's effects are therefore disregarded. Moreover, straight gooey damping with a coefficient c is accepted to be the damping in the framework. Furthermore, it is expected that the cantilever's neutral axis is inextensible.

The overseeing condition of movement for the cantilever beam can be acquired by applying the extended Hamilton variation principle, following a series of simplifications and taking into account the homogenous boundary conditions [14,52-54]:

$$\rho_{c}A_{c}v_{u} + cv_{t} + E_{c}I_{c}(v_{ssss} + v_{s}^{2}v_{ssss} + 4v_{s}v_{ss}v_{sss} + v_{ss}^{3})
- \rho_{c}A_{c}\left[v_{s}w_{tt} + v_{ss}\int_{L}^{s}w_{tt}d\zeta\right]
+ \frac{1}{2}\rho_{c}A_{c}\left[v_{s}\int_{0}^{s}(v_{y}^{2})_{tt}dy + v_{ss}\int_{L}^{s}\int_{0}^{\zeta}(v_{y}^{2})_{tt}dyd\zeta\right] - m\delta_{D}(s)
- L)\left[v_{s}w_{tt} + v_{ss}\int_{L}^{s}w_{tt}d\zeta\right]
+ \frac{1}{2}m\delta_{D}(s - L)\left[v_{s}\int_{0}^{s}(v_{y}^{2})_{tt}dy + v_{ss}\int_{L}^{s}\int_{0}^{\zeta}(v_{y}^{2})_{tt}dyd\zeta\right] = 0,$$
(1)

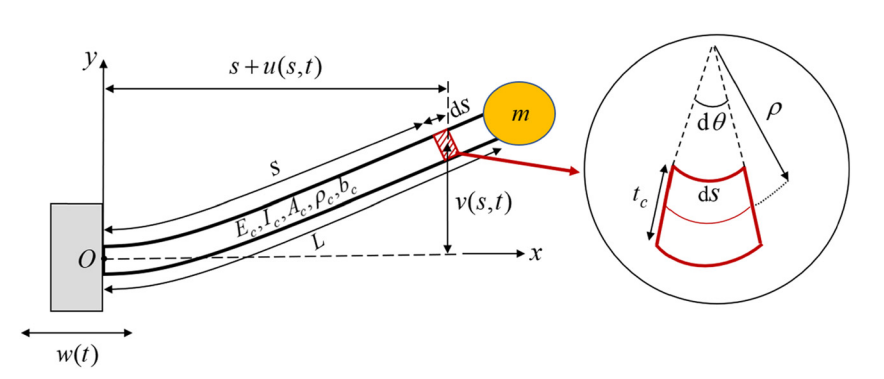


Figure 1: A parametrically energized cantilever framework with a tip mass.

where δ_D represents the Dirac delta function and the subscripts t and s symbolize the derivatives with respect to these variables, respectively. Presenting

$$Y = \sqrt{\frac{E_c I_c}{\rho_c A_c L^4}},\tag{2}$$

and the non-dimensional parameters

$$\hat{s} = \frac{s}{L}, \hat{v} = \frac{v}{L}, \hat{w} = \frac{w}{L}, \hat{v} = \frac{v}{L}, \hat{\zeta} = \frac{\zeta}{L}, \hat{t} = tY,$$

$$\hat{c} = \frac{c}{\rho_c A_c Y}, \hat{\omega}_0 = \frac{\omega_0}{Y}, \hat{m} = \frac{m}{\rho_c A_c L},$$
(3)

where ω_0 is the framework's lowest un-damped natural frequency. One way to express Equation (1) is in the dimensional form

There is no closed-form solution to the nonlinear governing differential Equation (4).

The transverse deflection $\hat{v}(\hat{s}, \hat{t})$ is anticipated by way of a direct mix of the commitments from N vibration modes in order to make a diminished request model for the parametrically energized cantilever. As a result, $\hat{v}(\hat{s}, \hat{t})$ can be expressed as [55], which is

$$\hat{v}(\hat{s}, \hat{t}) = \sum_{r=1}^{N} \psi_r(\hat{s}) Z_r(\hat{t}), \tag{5}$$

where $\psi_r(\hat{s})$ and $Z_r(\hat{t})$ are the direct mass-standardized mode shape capabilities for the Euler–Bernoulli cantilever pillar with a tip mass and the non-layered uprooting reaction of the rth vibration mode, individually. Depending simply on the principal vibration mode (N=1) in Equation (5) and disposing of addendum 1 for clarity, which turns out as expected when the excitation recurrence is essentially lower than the framework's second normal recurrence $\psi(\hat{s})$, is addressed as

$$\psi(\hat{s}) = R \, \bar{\psi}(\hat{s}), \tag{6}$$

where

$$R = \frac{1}{\sqrt{\int_0^1 (\bar{\psi}(\hat{s}))^2 \, \mathrm{d}\hat{s} + \hat{m}(\bar{\psi}(\hat{s}=1))^2}},$$
 (7)

$$\bar{\psi}(\hat{s}) = (\cos(\lambda \hat{s}) - \cosh(\lambda \hat{s})) + Q(\sin(\lambda \hat{s}) - \sinh(\lambda \hat{s})),$$
 (8)

$$Q = \frac{\sin(\lambda) - \sinh(\lambda) + \lambda \hat{m}(\cos(\lambda) - \cosh(\lambda))}{\cos(\lambda) + \cosh(\lambda) - \lambda \hat{m}(\sin(\lambda) - \sinh(\lambda))}.$$
 (9)

In Equations (8) and (9), the eigenvalue of the first vibration mode for which the relation holds is represented by

$$\lambda = \sqrt{\hat{\omega}_0} , \qquad (10)$$

Additionally, λ satisfies the characteristic equation

1 +
$$\cosh(\lambda) \cos(\lambda) + \hat{m}\lambda(\cos(\lambda)\sinh(\lambda)$$

- $\sin(\lambda)\cosh(\lambda)) = 0$, (11)

It is believed that the cantilever beam's clamped end moves axially in a harmonic manner with an acceleration amplitude a_p , *i.e.*, w_{tt} is symbolized by way of

$$w_{tt} = a_{\rm p} \cos(\Omega_{\rm p} t), \tag{12}$$

where $\Omega_{\rm p}$ is the parametric excitation frequency that has a non-dimensional expression

$$\hat{\Omega}_{\rm p} = \frac{\Omega_{\rm p}}{V}.\tag{13}$$

Consequently, taking into account Equation (3), the clamped's non-dimensional acceleration \hat{w}_{if} is calculated as

$$\hat{w}_{\hat{t}\hat{t}} = \hat{a}_{p} \cos(\hat{\Omega}_{p}\hat{t}), \tag{14}$$

where \hat{a}_p is the non-dimensional acceleration amplitude defined as

$$\hat{a}_{\rm p} = \frac{a_{\rm p}}{LV^2}.\tag{15}$$

Consequently, Equation (5) for the first vibration mode is inserted into Equation (4) to produce the final, reduced-order equation of motion for the system, which is then multiplied by $\psi(\hat{s})$ and integrated over the non-dimensional length as [56]

$$\ddot{Z} + \beta \dot{Z} + \hat{\omega}_0^2 (1 + P \cos(\hat{Q}_p \hat{t})) Z + \eta Z^3 + \alpha (\dot{Z}^2 + Z \ddot{Z}) Z$$
= 0, (16)

where the derivatives are with respect to \hat{t} , and β , P, η , and α are the coefficients of damping, parametric excitation amplitude, Duffing-type nonlinearity, and nonlinear inactivity term, respectively, which are characterized as

$$\beta = \hat{c}, P = \frac{h_2}{\hat{\omega}_0^2 h_1} \hat{a}_p, \eta = \frac{h_3}{h_1}, \alpha = \frac{h_4 + h_5}{h_1}, \tag{17}$$

where

$$h_1 = \int_0^1 \psi^2 d\hat{s}, h_2 = \int_0^1 ((1 - \hat{s})\psi\psi_{\hat{s}\hat{s}} - \psi\psi_{\hat{s}})d\hat{s} - \hat{m}\psi(1)\psi_{\hat{s}}(1),$$

$$h_{3} = \int_{0}^{1} \psi(\psi_{\hat{s}}^{2} \psi_{\hat{s}\hat{s}\hat{s}\hat{s}\hat{s}} + 4\psi_{\hat{s}} \psi_{\hat{s}\hat{s}} \psi_{\hat{s}\hat{s}\hat{s}} + \psi_{\hat{s}\hat{s}}^{2}) d\hat{s},$$

$$h_{4} = \int_{0}^{1} \psi \psi_{\hat{s}} \left(\int_{0}^{\hat{s}} (\psi_{\hat{y}}(\hat{y}))^{2} d\hat{y} d\hat{s} \right) d\hat{s},$$

$$h_{5} = \int_{0}^{1} \psi \psi_{\hat{s}\hat{s}} \left(\int_{0}^{\hat{s}} (\psi_{\hat{y}}(\hat{y}))^{2} d\hat{y} d\hat{s} \right) d\hat{s}.$$

This part produced the mathematical model for a PECB with a tip mass. In this section, we use the first-order approximation of the multiple time-scale technique to get approximate solutions for Equation (16). Equation (16) is scaled as follows, assuming that the system parameters counting β , P, η , and α to be minor and of a similar order ε

$$\ddot{Z} + \varepsilon \beta_{\varepsilon} \dot{Z} + \hat{\omega}_{0}^{2} (1 + \varepsilon P_{\varepsilon} \cos(\hat{Q}_{p} \hat{t})) Z + \varepsilon \eta_{\varepsilon} Z^{3}$$

$$+ \varepsilon \alpha_{\varepsilon} (\dot{Z}^{2} + Z \ddot{Z}) Z = 0.$$
(18)

where $\beta = \varepsilon \beta_{\varepsilon}$, $P = \varepsilon P_{\varepsilon}$, $\eta = \varepsilon \eta_{\varepsilon}$, $\alpha = \varepsilon \alpha_{\varepsilon}$.

3 Cantilever beams with various control kinds mathematically

After including several controllers, the improved model system Equation (18) was explored as follows [16]:

$$\ddot{Z} + \varepsilon \beta_{\varepsilon} \dot{Z} + \hat{\omega}_{0}^{2} (1 + \varepsilon P_{\varepsilon} \cos(\hat{\Omega}_{p} \hat{t})) Z + \varepsilon \eta_{\varepsilon} Z^{3}$$

$$+ \varepsilon \alpha_{\varepsilon} (\dot{Z}^{2} + Z \ddot{Z}) Z = F_{c}(t),$$
(19)

where $F_c(t)$ is the control input, and it can be stated as follows using different types of controls to lessen the vibrations that occur in the principal parametric resonance case $(\hat{Q}_p = 2\hat{\omega}_0)$ as follows:

First type: IRC

$$\dot{v}_1 + \sigma_{v_1} v_1 = \lambda_{v_1} Z
F_c(t) = \varepsilon k_{v_1} v_1.$$
(20)

Second type: PPF

$$\ddot{u}_1 + \varepsilon \mu_1 \, \dot{u}_1 + \omega_1^2 \, u_1 + \varepsilon \delta_1 \, u_1^3 = \varepsilon \lambda_{u_1} Z$$

$$F_c(t) = \varepsilon k_{u_1} \, u_1.$$
(21)

Third type: Nonlinear integral positive position feedback (NIPPF)

Fourth type: Nonlinear proportional-derivative (NPD) within NPDCVFC

$$\ddot{Z} + \varepsilon \beta_{\varepsilon} \dot{Z} + \hat{\omega}_{0}^{2} (1 + \varepsilon P_{\varepsilon} \cos(\hat{\Omega}_{p} \hat{t})) Z + \varepsilon \eta_{\varepsilon} Z^{3}$$

$$+ \varepsilon \alpha_{\varepsilon} (\dot{Z}^{2} + Z \ddot{Z}) Z = F_{c}(t),$$

$$E_{c}(t) = -\varepsilon (p_{c} Z + d_{c} \dot{Z} + q_{2} Z^{3} + q_{2} Z^{2} \dot{Z} + q_{2} Z \dot{Z}^{2} + G_{1} \dot{Z}^{3}).$$
(23)

where $-(p_1Z + d_1\dot{Z})$, is the linear control force, $-(\alpha_1Z^3 + \alpha_2Z^2\dot{Z} + \alpha_3Z\dot{Z}^2)$ is the non-linear control force, and G_1 , G_2 are the gains.

Since the fourth control kind is the most effective at suppressing vibrations in the worst resonance condition, we have only included it in this area of the mathematical study. Figure 2 displays the model with the controller under consideration.

3.1 Perturbation and stability analysis

The response is approximated as [57] in the first-order approximation of the multiple time scale

$$Z(\hat{t}, \varepsilon) = Z_0(T_0, T_1) + \varepsilon Z_1(T_0, T_1) + O(\varepsilon^2),$$
 (24)

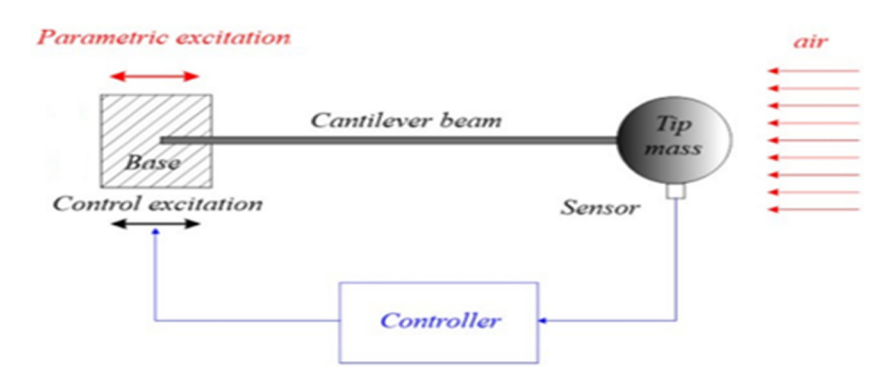


Figure 2: A schematic diagram model of the cantilever beam with excitation via new controller NPDCVFC.

where $T_0 = t$ and $T_1 = \varepsilon t$ represent time scales. Substituting Equation (24) into Equation (19) within Equation (23) and merely accepting the terms of the order $O(\varepsilon^0)$ and $O(\varepsilon^1)$ taking into consideration the equation's outcomes

$$\begin{split} D_0^2 Z_0 + \varepsilon (D_0^2 Z_1 + 2D_0 D_1 Z_0) + \varepsilon (D_0^2 Z_1 + 2D_0 D_1 Z_0) \\ + \varepsilon \beta_{\varepsilon} (D_0 Z_0) + \varepsilon \eta_{\varepsilon} Z_0^3 \\ + \hat{\omega}_0^2 (1 + \varepsilon P_{\varepsilon} \cos(\hat{Q}_p \hat{t})) (Z_0 + \varepsilon Z_1) \\ + \varepsilon \alpha_{\varepsilon} Z_0 ((D_0 Z_0)^2 + Z_0 (D_0^2 Z_0)) \\ + \varepsilon \left[p_1 (Z_0 + \varepsilon Z_1) + d_1 (D_0 Z_0) + \alpha_1 (Z_0^3) \\ + \alpha_2 ((Z_0 + \varepsilon Z_1)^2 (D_0 Z_0)) \\ + \alpha_3 Z_0 (D_0 Z_0)^2 + G_1 (D_0 Z_0)^3 \right] = 0, \end{split}$$

Wherever, the derivatives are with respect to \hat{t} . Associating terms of the same order of ε in Equation (25) yields

$$O(\varepsilon^0)$$
: $(D_0^2 + \hat{\omega}_0^2)Z_0 = 0$, (26)

$$\begin{split} O(\varepsilon^{1}) &: (D_{0}^{2} + \hat{\omega}_{0}^{2})Z_{1} \\ &= -2D_{0}D_{1}Z_{0} - \beta_{\varepsilon}D_{0}Z_{0} - \eta_{\varepsilon}Z_{0}^{3} - \alpha_{\varepsilon}Z_{0}(D_{0}Z_{0})^{2} \\ &- \alpha_{\varepsilon}Z_{0}^{2}D_{0}^{2}Z_{0} - \frac{1}{2}\hat{\omega}_{0}^{2}P_{\varepsilon}(e^{i\hat{\Omega}_{p}T_{0}} + e^{-i\hat{\Omega}_{p}T_{0}})Z_{0} - p_{1}Z_{0} . \end{split}$$
 (27)
$$- d_{1}(D_{0}Z_{0}) - \alpha_{1}Z_{0}^{3} - \alpha_{2}Z_{0}^{2}(D_{0}Z_{0}) - \alpha_{3}Z_{0} (D_{0}Z_{0})^{2} \\ - G_{1}(D_{0}Z_{0})^{3} \end{split}$$

The solution for Equation (26) is stated in the form

$$Z_0 = A(T_1) e^{i\hat{\omega}_0 T_0} + cc.$$
 (28)

Substituting Equation (28) into Equation (27) yields

$$(D_0^2 + \hat{\omega}_0^2)Z_1$$

$$= \begin{pmatrix} -2i\hat{\omega}_{0}D_{1}A - i\hat{\omega}_{0}\beta_{\varepsilon}A - \frac{1}{2}\hat{\omega}_{0}^{2}P_{\varepsilon}\bar{A}e^{i(\hat{Q}_{p}-2\hat{\omega}_{0})T_{0}} \\ -3\eta_{\varepsilon}A^{2}\bar{A} + 2\alpha_{\varepsilon}\hat{\omega}_{0}^{2}A^{2}\bar{A} - p_{1}A - i\hat{\omega}_{0}d_{1}A \\ -3\alpha_{1}A^{2}\bar{A} - 3i\alpha_{2}A^{2}\bar{A} - \alpha_{3}\hat{\omega}_{0}^{2}A^{2}\bar{A} \\ -3iG_{1}\hat{\omega}_{0}^{3}A^{2}\bar{A} \end{pmatrix} e^{i\hat{\omega}_{0}T_{0}}$$
(29)
+ NST + cc,

where cc stands for the complex conjugate of the preceding terms and NST denotes non-secular terms. Taking into account the principal parametric resonance scenario $\hat{\Omega}_p = 2\hat{\omega}_0$, the frequency detuning parameter $\hat{\sigma}_p$ for the parametric excitation frequency is characterized by way of

$$\hat{\Omega}_{\rm p} - 2\hat{\omega}_0 = \varepsilon \hat{\sigma}_{\rm p}. \tag{30}$$

The solvability conditions in Equation (29) produce when terms that produce secular terms are rejected using Equation (30). Considering Equation (30), eliminating the secular terms in Equation (29) yields

$$2i\hat{\omega}_{0} D_{1} A + i\hat{\omega}_{0}\beta_{\varepsilon}A + \frac{1}{2}\hat{\omega}_{0}^{2}P_{\varepsilon} \bar{A}e^{i\hat{\sigma}_{p}T_{1}} - 3\eta_{\varepsilon}A^{2}\bar{A}$$

$$+ 2\alpha_{\varepsilon}\hat{\omega}_{0}^{2}A^{2}\bar{A} - p_{1}A - i\hat{\omega}_{0}d_{1}A$$

$$- 3\alpha_{1}A^{2}\bar{A} - 3i\alpha_{2}A^{2}\bar{A} - \alpha_{3}\hat{\omega}_{0}^{2}A^{2}\bar{A} - 3iG_{1}\hat{\omega}_{0}^{3}A^{2}\bar{A} = 0.$$
(31)

To separate the averaging conditions that administer the elements of Equation (31), let express A and \bar{A} are exposed in the next polar formulas

$$A = \frac{1}{2}a(T_1)\exp[i\theta(T_1)], \quad \bar{A} = \frac{1}{2}a(T_1)\exp[-i\theta(T_1)], \quad (32)$$

where a and θ are the steady-state amplitudes and phases, respectively. Changing Equation (32) hooked on Equation (31), we obtain

$$-i\hat{\omega}_{0}a' - \frac{1}{2}\hat{\omega}_{0}a(\hat{\sigma}_{p} - \gamma') + \frac{1}{2}i\hat{\omega}_{0}\beta_{\varepsilon}a + \frac{1}{4}\hat{\omega}_{0}^{2} a P_{\varepsilon} (\cos \gamma)$$

$$+ i \sin \gamma) - \frac{3}{8}\eta_{\varepsilon}a^{3} + \frac{2}{8}\alpha_{\varepsilon}\hat{\omega}_{0}^{2}a^{3} - \frac{1}{2}p_{1}a$$

$$- \frac{1}{2}i\hat{\omega}_{0}d_{1}a - \frac{3}{8}\alpha_{1}a^{3} - \frac{3}{8}i\alpha_{2}a^{3} - \frac{1}{8}\alpha_{3}\hat{\omega}_{0}^{2}a^{3}$$

$$- \frac{3}{8}iG_{1}\hat{\omega}_{0}^{3}a^{3} = 0,$$
(33)

where $y = \hat{\sigma}_p T_1 - 2\theta$, separating real and imaginary elements, we obtain

$$a' = \frac{1}{2} \left[d_1 - \beta_{\varepsilon} - \frac{1}{2} \hat{\omega}_0 P_{\varepsilon} \sin \gamma \right] a + \frac{3}{8} \left[\frac{\alpha_2}{\hat{\omega}_0} + G_1 \hat{\omega}_0^2 \right] a^3, (34)$$

$$a\gamma' = \left[\hat{\sigma}_{p} - \frac{1}{2}\hat{\omega}_{0}P_{\varepsilon}\cos\gamma + \frac{p_{1}}{\hat{\omega}_{0}}\right]a + \frac{1}{4}\left[\frac{3}{\hat{\omega}_{0}}\eta_{\varepsilon} - 2\hat{\omega}_{0}\alpha_{\varepsilon} + \frac{3}{\hat{\omega}_{0}}\alpha_{1} + \alpha_{3}\hat{\omega}_{0}\right]a^{3}.$$
(35)

For steady-state responses (a' = y' = 0), the periodic solution corresponding to Equations (34) and (35) is given by

$$\left[d_1 - \beta_{\varepsilon} - \frac{1}{2}\hat{\omega}_0 P_{\varepsilon} \sin \gamma\right] a + \frac{3}{4} \left[\frac{\alpha_2}{\hat{\omega}_0} + G_1\hat{\omega}_0^2\right] a^3 = 0, (36)$$

$$\left[\hat{\sigma}_{p} - \frac{1}{2}\hat{\omega}_{0}P_{\varepsilon}\cos\gamma + \frac{p_{1}}{\hat{\omega}_{0}}\right]a + \frac{1}{4}\left[\frac{3}{\hat{\omega}_{0}}\eta_{\varepsilon} - 2\hat{\omega}_{0}\alpha_{\varepsilon} + \frac{3}{\hat{\omega}_{0}}\alpha_{1} + \alpha_{3}\hat{\omega}_{0}\right]a^{3} = 0.$$

$$(37)$$

Subsequently, the steady-state responses can be derived from the algebraic equations by the use of the Newton–Raphson approach and MATLAB software. The stability of the steady-state shell system is assessed by finding the right-hand side eigenvalues of the Jacobian matrix at Equations (34) and (35) using the Lyapunov first approach

$$\begin{bmatrix} a' \\ \gamma' \end{bmatrix} = \begin{bmatrix} R_{11} & R_{12} \\ R_{21} & R_{22} \end{bmatrix} \begin{bmatrix} a \\ \gamma \end{bmatrix},$$
 (38) Then,
$$\lambda^2 + \rho_1 \lambda + \rho_2 = 0,$$
 (40)

where

$$\begin{split} R_{11} &= \frac{\partial a'}{\partial a} = \frac{1}{2} \Big[d_1 - \beta_{\varepsilon} - \frac{1}{2} \hat{\omega}_0 P_{\varepsilon} \sin \gamma \Big] + \frac{9}{8} \Big[\frac{\alpha_2}{\hat{\omega}_0} + G_1 \hat{\omega}_0^2 \Big] a^2, \\ R_{12} &= \frac{\partial a'}{\partial \gamma} = -\frac{1}{4} \hat{\omega}_0 a P_{\varepsilon} \cos \gamma \\ R_{21} &= \frac{\partial \gamma'}{\partial a} = \frac{1}{a} \Big[\hat{\sigma}_p - \frac{1}{2} \hat{\omega}_0 P_{\varepsilon} \cos \gamma + \frac{p_1}{\hat{\omega}_0} \Big] \\ &+ \frac{3}{4} \Big[\frac{3}{\hat{\omega}_0} \eta_{\varepsilon} - 2 \hat{\omega}_0 \alpha_{\varepsilon} + \frac{3}{\hat{\omega}_0} \alpha_1 + \alpha_3 \hat{\omega}_0 \Big] a, \\ R_{22} &= \frac{\partial \gamma'}{\partial \gamma} = \frac{1}{2} \hat{\omega}_0 P_{\varepsilon} \sin \gamma \end{split}$$

The following determinant in the preceding matrix must be solved in order to determine the stable regions of the controlled model

$$\begin{vmatrix} R_{11} - \lambda & R_{12} \\ R_{21} & R_{22} - \lambda \end{vmatrix} = 0.$$
 (39)

where λ indicates the Jacobian matrix's eigenvalue, $\rho_1 = -R_{11} - R_{22}$ and $\rho_2 = R_{11}R_{22} - R_{12}R_{21}$. The Routh–Hurwitz criteria state that the following are $\rho_1 > 0$, and $\rho_2 > 0$, necessary and sufficient requirements for the structure to be stable. If the real parts of the eigenvalues are negative, the system is stable; if not, it is unstable. In frequency response curves, stable and unstable periodic responses are represented by solid and dotted lines, respectively.

3.2 Experimental model study

A vibration controller, power amplifier, shaker, cantilever beam, signal analyzer, data collection computer, and two accelerometers make up the experimental apparatus are used to conduct the studies. This configuration, which uses

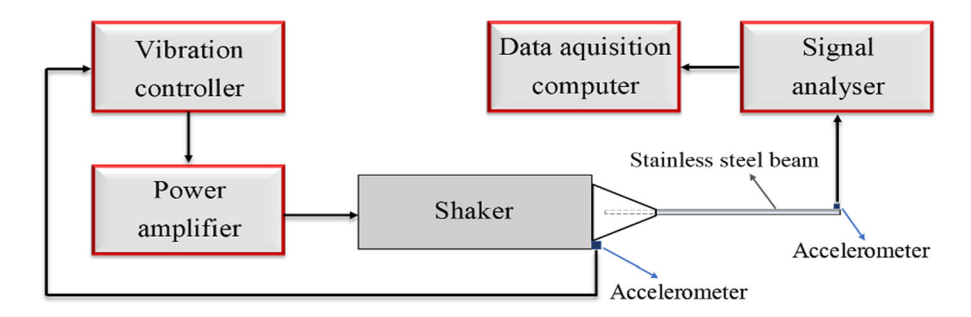


Figure 3: An experimental set-up schematic block design.



Figure 4: Design of a parametrically energized cantilever framework with a tip mass.

the novel controller NPDCVFC, is roughly block diagrammed in Figure 3 and illustrated in Figure 4 as described in Aghamohammadi *et al.* [16]. The numerical results and their corresponding numerical outcomes are presented in the following section.

4 Outcomes and simulation discussions

4.1 Numerical simulation with time history

Equations (19)–(23) just illustrated the nonlinear dynamical structure. Four different types of control techniques (IRC–PPF–NIPPF–NPDCVFC) were then attached, and the 0 18.0 computer programmer was used to numerically simulate them in order to determine which control would minimize the oscillations in the model. The time history of Figures 5–9 is used to illustrate the parameter values as follows:

$$\begin{split} \beta_{\varepsilon} &= 0.2, \, \hat{\omega}_0 = 1.5, \, P_{\varepsilon} = 2.15, \, \hat{\mathcal{Q}}_{\mathrm{p}} = 2\hat{\omega}_0, \, \eta_{\varepsilon} = 1.15, \, \alpha_{\varepsilon} = 1.02, \\ \sigma_{v_1} &= 0.66, \\ \lambda_{v_1} &= 0.7, \, k_{v_1} = 0.5, \, \mu_1 = 2.0, \, \omega_1 = 1.6, \, \delta_1 = 0.5, \, \lambda_{u_1} = 1.75 k_{u_1} \\ &= 0.4, \\ p_1 &= 0.2, \, d_1 = 0.3, \, \alpha_1 = 0.4, \, \alpha_2 = 0.35, \, \alpha_3 = 0.74, \, G_1 = 3.6, \\ \varepsilon &= 0.25 \end{split}$$

and zero initial conditions. Figure 5 has attained the basic steady-state amplitude Z(t) before starting any controller at the principal parametric resonance item $\hat{\Omega}_{\rm p}=2\hat{\omega}_0$ as the worst resonance case of the system. The outcomes for adding the controllers (IRC, PPF, NIPPF, and NPDCVFC) are displayed in Figures 6–9, allowing you to choose the most effective way to lower the high vibration amplitudes.

Based on Figures 6–9, we may conclude that the new controller NPDCVFC is the best. This section discusses the construction of the controller for the active vibration of the measured cantilever beam is covered in this section (Figure 9). As mentioned earlier, NPD and the NCVFC algorithm are used to provide active vibration control. For this structural

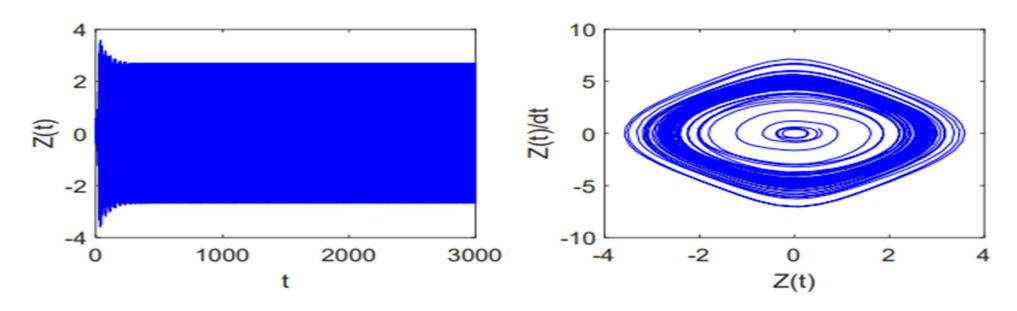


Figure 5: Uncontrolled framework vibration amplitude on the measured principal parametric resonance case $(\hat{\Omega}_p = 2\hat{\omega}_0)$.

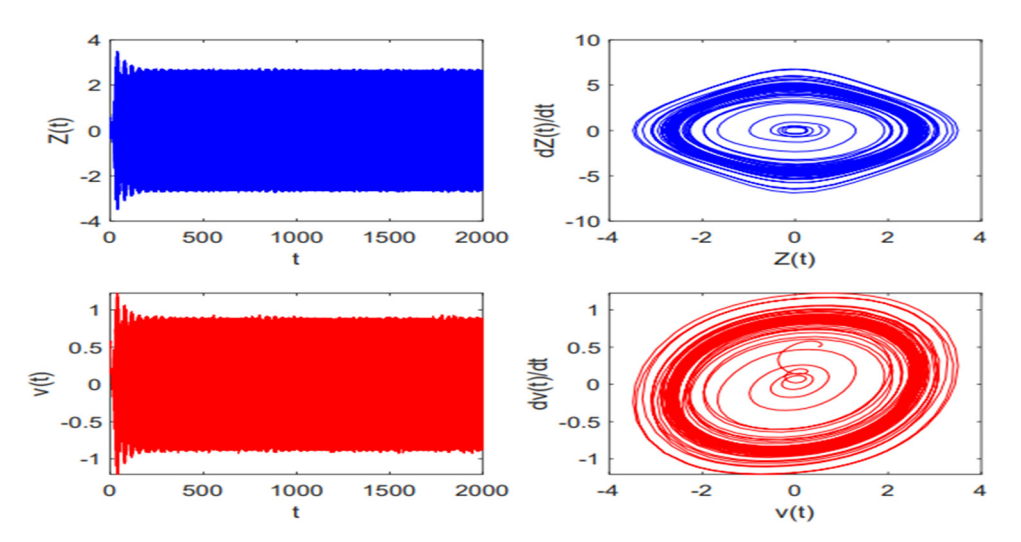


Figure 6: Controlled structure vibration amplitude inside the measured principal parametric resonance item $(\hat{Q}_p = 2\hat{\omega}_0)$ via IRC.

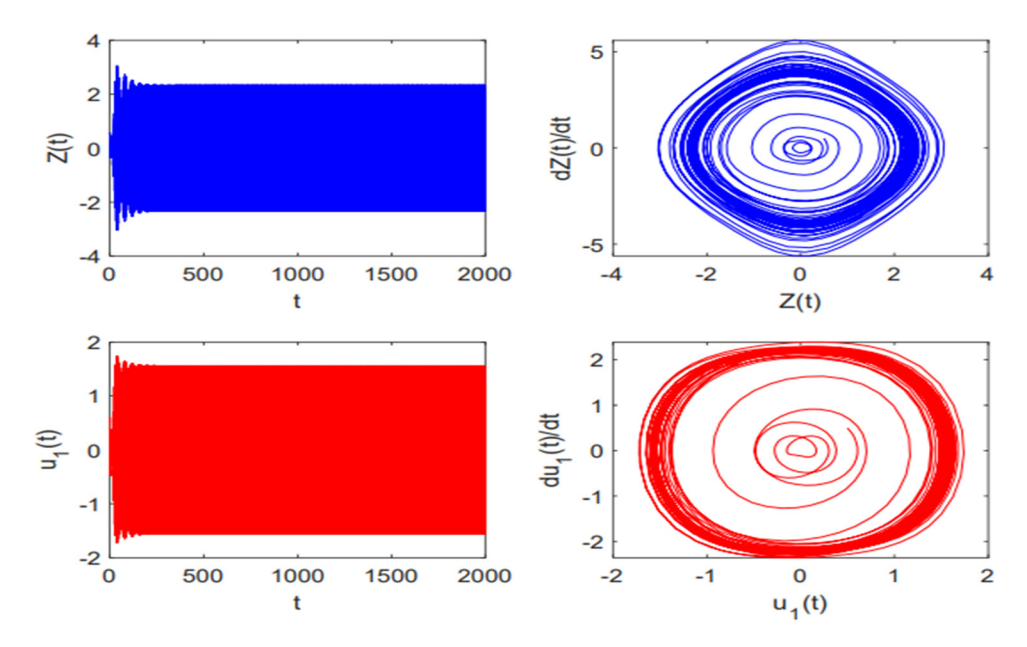


Figure 7: Controlled framework oscillation amplitude at the restrained principal parametric resonance case $(\hat{\mathcal{Q}}_p = 2\hat{u}_0)$ applying PPF.

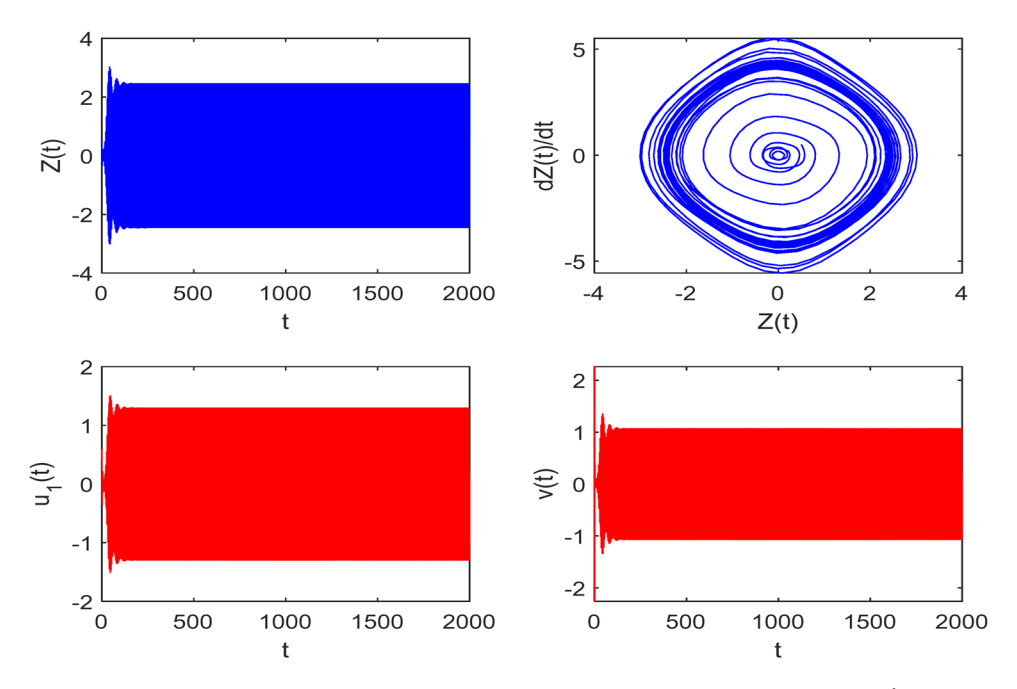


Figure 8: Controlled structure vibration amplitude organized on the dignified principal parametric resonance item ($\hat{\mathcal{Q}}_{\mathrm{p}}$ = $2\hat{\omega}_{\mathrm{0}}$) via NIPPF.

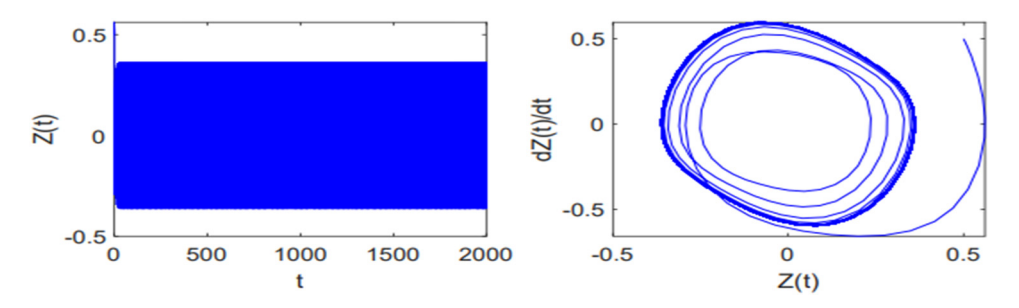


Figure 9: Controlled framework vibration amplitude concluded the measured principal parametric resonance item ($\hat{\mathcal{Q}}_{p}$ = $2\hat{\omega}_{0}$) *via* NPDCVFC.

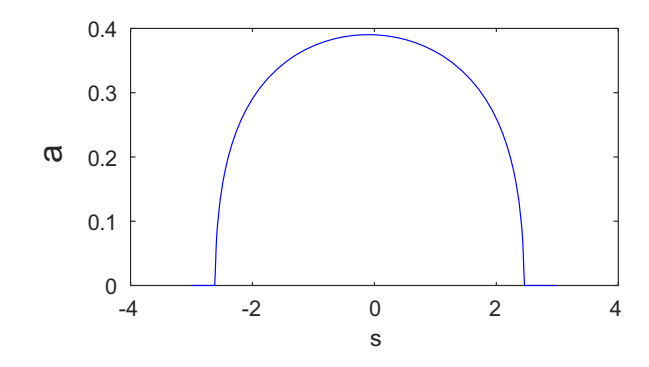


Figure 10: Influence response curves a versus σ of the controlled system.

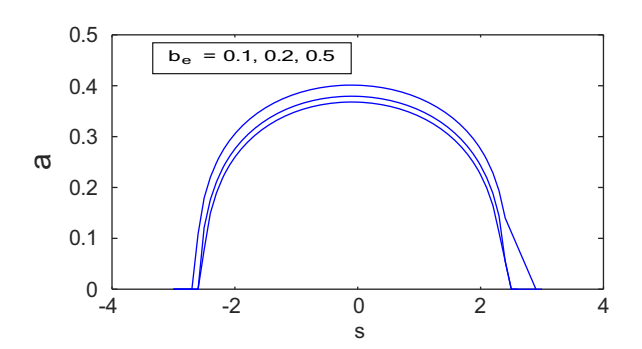


Figure 11: Impact of damping coefficient β_{ε} .

model, the depreciation rate features are enhanced by this controller rule. It is evident that this straightforward strategy may work well for reducing the infinite norm of vibration amplitudes. The findings demonstrate the effectiveness of the optimization strategy in reducing vibrations and the speed at which vibrations in the measured cantilever beam were suppressed by angularly orienting actuators and sensors in the proper places. Thus, in order to explore the controlled model and examine the acts of different controlled parameters on the framework, we shall select and statistically evaluate it.

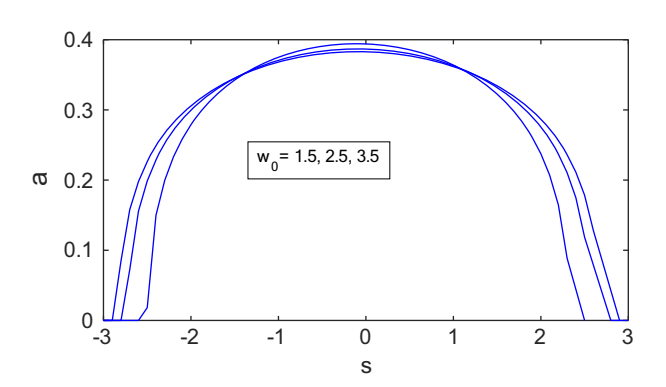


Figure 12: Effect of excitation frequency $\hat{\omega}_0$.

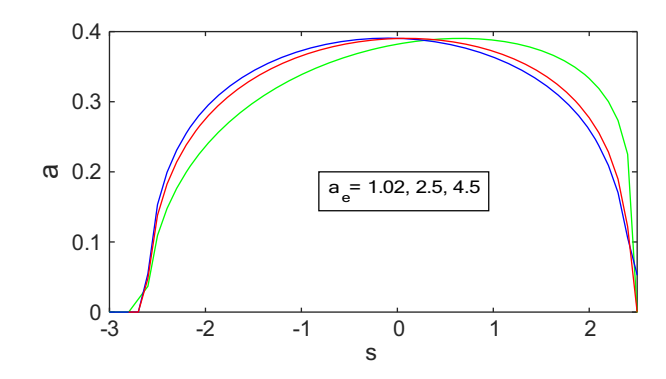


Figure 13: Influence of nonlinear coefficient α_{ε} .

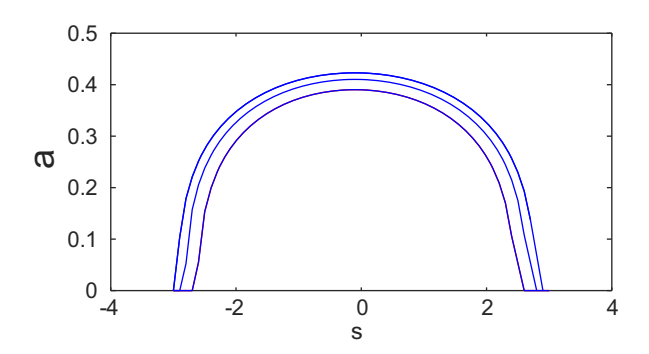


Figure 14: Influence of parametric force coefficient P_{ε} = 3.5, 2.15, 1.5.

4.2 Simulation of stability and the impact of different regulated model coefficients

This section investigated the influence of various parameters on the controlled structure in Equations (36)–(40) besides numerically demonstrated stable and un-stable regions. The helpful case $a_1 \neq 0$, $a_2 \neq 0$ is investigated in order to obtain a large number of parameter impacts. As can be seen in Figures 10–18, all curves exhibit only stable sections with no instability zonoutcome for any vibrating

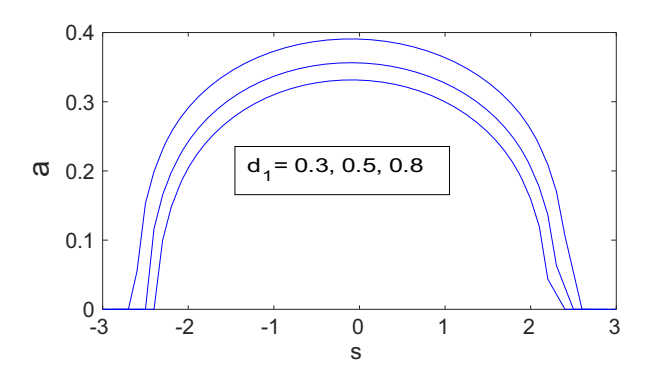


Figure 15: Influence of the linear control force coefficient d_1 .

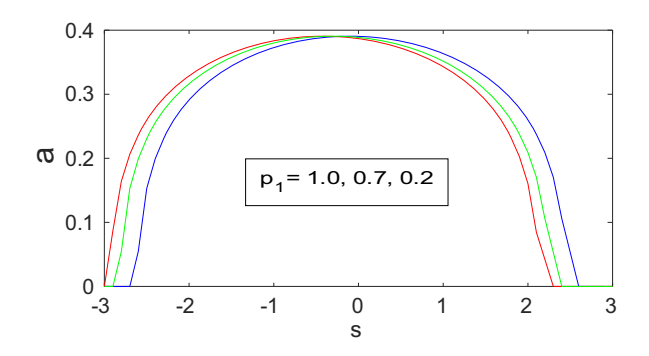


Figure 16: Influence of the linear control force coefficient p_1 .

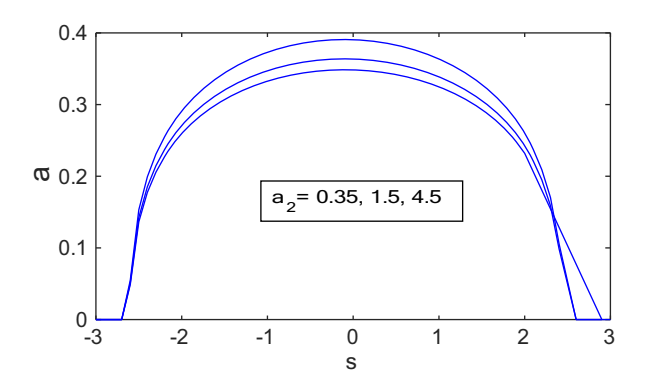


Figure 17: Influence of nonlinear control parameter α_2 .

systemes when NPDCVFC is indicated to the system. This is another justification for adding this additional controller to the structure, which is a desirable outcome for any vibrating system. Solid curves reflect responses that are stable. The solid line represents the stability regions shown graphically by (______). Figure 10 depicts the performance of the amplitude–frequency response steady-state response curves. As illustrated in Figure 10, the backbone curve is acquired as a basic case of a against which shows stable region with no instability zones. As damping coefficient β_{ε} decreased the amplitude a is increased and the stability

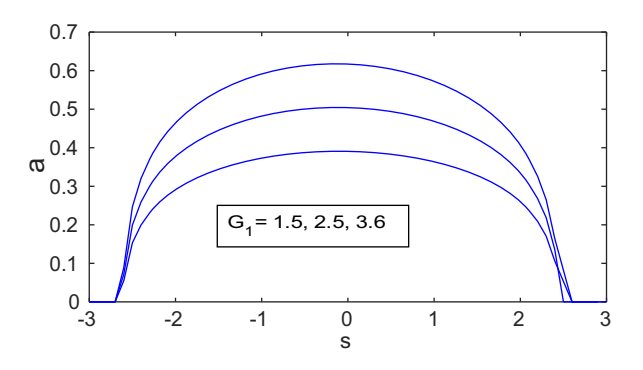


Figure 18: Influence of nonlinear control gain G_1 .

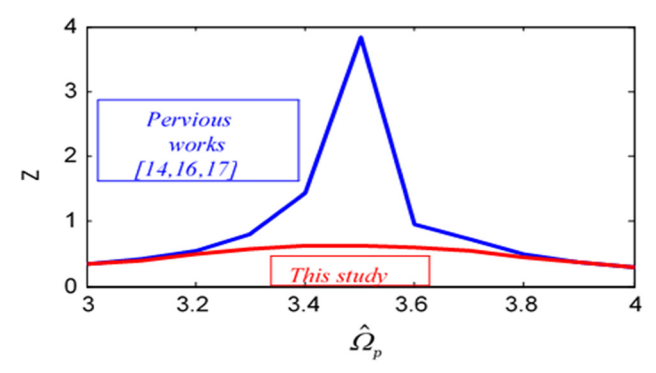


Figure 19: A comparison of the current work's results with those from earlier studies [14.16,17] both with and without a controller.

region is increased as appeared in Figure 11. By way of the excitation frequency $\hat{\omega}_0$ is increased the steady-state amplitude a is decreased and all regions are stable as shown in Figure 12. Moreover, the diagrams of the nonlinear coefficient α_c is shifted to right when the values are increased with no instability regions as depicted in Figure 13. Also, as the parametric force coefficient P_{ε} is increased the steady-state amplitude a increased with increasing in stability regions as displayed in Figure 14. On the other hand, when the linear control force coefficient d_1 increased the steady-state amplitude a has decreased and all regions are stable as plotted in Figure 15. Besides, the curve of the linear control force coefficient p_1 is shifted to right (S.R) when the values of parameter p_1 are increased with no instability regions as described in Figure 16. Also, as shown in Figure 17, the values of the nonlinear control parameter α_2 is decreased when the amplitude is increased with increasing the stable regions. In the last, as the gain coefficient G_1 increased the steady-state amplitude a_1 be small with stability regions as presented in Figure 18.

4.3 Comparison of the same model with more recent studies

A parametrically energized cantilever beam (PECB) with a tip mass model system akin to Equation (18) was examined in previous studies [14,16,17]. However, they applied the multiple time-scale process within the principal parametric resonance item to study the behavior of the structure under mixed parametric and harmonic excitations, eliminating the need for a controller. The development of the model given by Aghamohammadi *et al.* [16] is examined in the current work. I add a variety of control strategies to the vibrating structure system's modified system in order to determine which one reduces the framework structure's risk of vibration. Additionally, the upgraded system's new controller

(NPDCVFC) is examined in this article. The results of this research show that the novel controller less than the other controllers decreases the high vibrational amplitude of the model exposed to parametric stimulation inside the principal parametric resonance, as shown in Section 4.1. The perturbation approach is used to aid in the acquisition of analytical solutions. Plotting of the frequency response graphs occurs at different framework parameter levels. We end with a numerical validation of the obtained results. The comparisons show that the current approach produces findings that are remarkably similar to those found in Aghamohammadi *et al.* [16] and that the discrepancies are less than 1%. The influence response on recent works [14,16,17] with and without a controller is also compared to the current study's NPDCVFC controller, as displayed in Figure 19.

5 Conclusion

This work aims to present a new controller, NPDCVFC, that operates on (PECB) with a model of the tip mass. To raise the nonlinear coefficients, it blends NPD with the inclusion of NCVFC. The perturbation strategy is suitable for approximating the solution of the considered controlled model. The item that is regarded as the worst is the primary parametric resonance item ($\hat{\Omega}_p = 2\hat{\omega}_0$). To determine which controller design method reduces high amplitude vibrations at the major parametric resonance case the best, a comparison of several controller design methods (PPF control, NIPPF control, IRC control, and NPDCVFC as novel control techniques) has been made. It has been shown that the novel controller, NPDCVF, is very effective in reducing vibrations in the structure close to the resonance case under consideration. For every frequency response curve, the unstable and stable zones were obtained through the execution of a numerical stability study. The numerical clarification of the model's amplitude variation inside frequency response curves under the new controller has been considered. The results demonstrate how remarkably well the unique measured controller lowers the vibrations of the system under investigation. The lack of zones of instability in the response curves is another unique result of the novel controller that has been demonstrated. Numerical research has been done on the impacts and implications of each coefficient on the changed controlled system inside the frequency response curves.

Acknowledgment: The author extends his appreciation to Prince Sattam bin Abdulaziz University for funding this research work through Project number PSAU/2023/01/25363.

Funding information: This work was supported by Prince Sattam bin Abdulaziz University in Alkharj (Grant No. PSAU/2023/01/25363).

Author contributions: The author confirms the sole responsibility for the conception of the study, presented results and manuscript preparation.

Conflict of interest: The author states no conflict of interest.

Data availability statement: All data generated or analyzed during this study are included in this published article.

References

- [1] Kang HJ, Guo T, Zhu WD. Analysis on the in-plane 2: 2: 1 Internal resonance of a complex cable-stayed bridge system under external harmonic excitation. J Comput Nonlinear Dyn. 2021;16:101001, (1–15).
- [2] Liu M, Zheng L, Zhou P, Xiao H. Stability and dynamics analysis of in-plane parametric vibration of stay cables in a cable-stayed bridge with superlong spans subjected to axial excitation. J Aerosp Eng. 2020;33(1):04019106.
- [3] Hikami Y, Shiraishi N. Rain-wind induced vibrations of cables in cable stayed bridges. J Wind Eng Ind Aerodyn. 1988;29:409–18.
- [4] El Ouni MH, Kahla NB, Preumont A. Numerical and experimental dynamic analysis and control of a cable stayed bridge under parametric excitation. Eng Struct. 2012;45:244–56.
- [5] Lu Q, Sun Z, Zhang W. Nonlinear parametric vibration with different orders of small parameters for stayed cables. Eng Struct. 2020;224:111198.
- [6] Virlogeux M. State-of-the-art in cable vibrations of cable stayed bridges. Bridge Struct. 2005;1(3):133–68.
- [7] Parker RG, Wu X. Parametric instability of planetary gears having elastic continuum ring gears. J Vib Acoust. 2012;134(4):041011, (1–11).
- [8] Yildirim T, Ghayesh MH, Li W, Alici G. Design and development of a parametrically excited nonlinear energy harvester. Energy Convers Manage. 2016:126:247–55.
- [9] Rhoads JF, Kumar V, Shaw SW, Turner KL. The non-linear dynamics of electromagnetically actuated micro beam resonators with purely parametric excitations. Int J Non-Linear Mech. 2013;55:79–89.
- [10] Genter S, Paul O. Parylene-C as an electret material for micro energy harvesting. Doctoral dissertation, Universität Freiburg: 2019.
- [11] Mbong TD, Siewe MS, Tchawoua C. Controllable parametric excitation effect on linear and nonlinear vibrational resonances in the dynamics of a buckled beam. Commun Nonlinear Sci Numer Simul. 2018;54:377–88.
- [12] Bajaj A, Chang S, Johnson J. Amplitude modulated dynamics of a resonantly excited auto parametric two degree-of-freedom system. Nonlinear Dyn. 1994;5(4):433–57.

- [13] Zhang A, Sorokin V, Li H. Energy harvesting using a novel auto parametric pendulum absorber-harvester. J Sound Vib. 2021;499:116014.
- [14] Kumar V, Miller JK, Rhoads JF. Nonlinear parametric amplification and attenuation in a base-excited cantilever beam. J Sound Vib. 2011;330(22):5401-9.
- [15] Zaghari B, Rustighi E, Tehrani MG. Phase dependent nonlinear parametrically excited systems. J Vib Control. 2019;25(3):497-505.
- [16] Aghamohammadi M, Sorokin V, Mace B. Nonlinear dynamics of parametrically excited cantilever beams with a tip mass considering nonlinear inertia and duffing-type nonlinearity. Nonlinear Dyn. 2023;111:7251-69.
- [17] Zhang W, Wang F, Yao M. Global bifurcations and chaotic dynamics in nonlinear nonplanar oscillations of a parametrically excited cantilever beam. Nonlinear Dyn. 2005;40(3):251-79.
- [18] Han Q, Wang J, Li Q. Experimental study on dynamic characteristics of linear parametrically excited system. Mech Syst Signal Process. 2011;25(5):1585-97.
- [19] Lee Y, Pai PF, Feng Z. Nonlinear complex response of a parametrically excited tuning fork. Mech Syst Signal Process. 2008;22(5):1146-56.
- [20] Liu K, Deng L. Identification of pseudo-natural frequencies of an axially moving cantilever beam using a subspace-based algorithm. Mech Syst Signal Process. 2006;20(1):94-113.
- Harish KM, Gallacher BJ, Burdess JS, Neasham JA. Experimental investigation of parametric and externally forced motion in resonant MEMS sensors. J Micromech Microeng. 2008;19(1):015021.
- [22] Oropeza-Ramos LA, Burgner CB, Turner KL. Robust micro-rate sensor actuated by parametric resonance. Sens Actuators A. 2009;152(1):80-7.
- [23] Pallay M, Daeichin M, Towfighian S. Feasibility study of a MEMS threshold-pressure sensor based on parametric resonance: Experimental and theoretical investigations. J Micromech Microeng. 2020;14(8):1-10.
- [24] Zhang W, Baskaran R, Turner KL. Effect of cubic nonlinearity on auto-parametrically amplified resonant MEMS mass sensor. Sens Actuators A. 2002;102(1-2):139-50.
- [25] Mao XY, Ding H, Chen LQ. Parametric resonance of a translating beam with pulsating axial speed in the supercritical regime. Mech Res Commun. 2016;76:72-7.
- [26] Rhoads JF, Shaw SW, Foster KL, Moehlis J. Generalized parametric resonance in electrostatically actuated microelectromechanical oscillators. J Sound Vib. 2006;296(4-5):797-829.
- [27] Rhoads JF, Shaw SW, Turner KL. The nonlinear response of resonant microbeam systems with purely parametric electrostatic actuation. J Micromech Microeng. 2006;16(5):890-9.
- [28] Siewe MS, Tchawoua C, Rajasekar S. Parametric resonance in the Rayleigh-Duffing oscillator with time-delayed feedback. Commun Nonlinear Sci Numer Simul. 2012;17(11):4485-93.
- [29] Aghamohammadi M, Sorokin V, Mace B. On the response attainable in nonlinear parametrically excited systems. Appl Phys Lett. 2019;115(15):154102.
- [30] Chen S, Epureanu B. Forecasting bifurcations in parametrically excited systems. Nonlinear Dyn. 2018;91(1):443-57.
- [31] Warminski J. Nonlinear dynamics of self-, parametric, and externally excited oscillator with time delay: van der Pol versus Rayleigh models. Nonlinear Dyn. 2020;99(1):35-56.

- [32] Warminski J. Frequency locking in a nonlinear MEMS oscillator driven by harmonic force and time delay. Int J Dyn Control. 2015;3(2):122-36.
- [33] Li D, Shaw SW. The effects of nonlinear damping on degenerate parametric amplification. Nonlinear Dyn. 2020;102(4):2433-52.
- [34] Zaitsev S, Shtemppluck O, Buks E, Gottlieb O. Nonlinear damping in a micromechanical oscillator. Nonlinear Dyn. 2012;67(1):859-83.
- [35] Gutschmidt S. Gottlieb O. Nonlinear dynamic behavior of a microbeam array subject to parametric actuation at low, medium and large DC-voltages. Nonlinear Dyn. 2012;67(1):1-36.
- [36] Nayfeh AH, Mook DT, Holmes P. Nonlinear oscillations. New York: Wiley inter science; 1980.
- [37] El-Sayed AT, Bauomy HS. Outcome of special vibration controller techniques linked to a cracked beam. Appl Math Model. 2018:63:266-87
- [38] El-Sayed AT, Bauomy HS. A beam-ring circular truss antenna restrained by means of the negative speed feedback procedure. | Vib Cont. 2022;28:2032-51.
- [39] El-Sayed AT, Bauomy HS. NIPPF versus ANIPPF controller outcomes on semi-direct drive cutting transmission system in a shearer. Chaos Sol Fract. 2022;156:111778, (1-19).
- Bauomy HS, El-Sayed AT. Vibration performance of a vertical conveyor system under two simultaneous resonances. Archive Appl Mech. 2018;88:1349-68.
- [41] Bauomy HS, El-Sayed AT. A new six-degrees of freedom model designed for a composite plate through PPF controllers. Appl Math Model. 2020;88:604-30.
- Bauomy HS, El-Sayed AT. Act of nonlinear proportional derivative controller for MFC laminated shell. Phys Scr. 2020;95:095210.
- Bauomy HS, El-Sayed AT. Mixed controller (IRC + NSC) involved in [43] the harmonic vibration response cantilever beam model. Meas Control. 2020;53:1954-67.
- Bauomy HS, El-Sayed AT. Nonlinear saturation controller simulation for reducing the high vibrations of a dynamical system. Math Biosci Eng. 2022;19:3487-508.
- [45] Bauomy HS. New controller (NPDCVF) outcome of FG cylindrical shell structure. Alex Eng J. 2021;61:1779-1801.
- Saeed NA, El-Bendary SI, Sayed M, Mohamed MS, Elagan SK. On the oscillatory behaviours and rub-impact forces of a horizontally supported asymmetric rotor system under positionvelocity feedback controller. Lat Am J Solids Struct. 2021;18(2):1-28, e349.
- [47] Saeed NA, Omara OM, Sayed M, Awrejcewicz J, Mohamed MS. Nonlinear interactions of jeffcott-rotor system controlled by a radial PD-control algorithm and eight-pole magnetic bearings actuator. Appl Sci. 2022;12(13):6688.
- [48] Saeed NA, Omara OM, Sayed M, Awrejcewicz J, Mohamed MS. On the rub-impact force, bifurcations analysis, and vibrations control of a nonlinear rotor system controlled by magnetic actuator integrated with PIRC-control algorithm. SN Appl Sci.
- Kandil A, Eissa M. Improvement of positive position feedback [49] controller for suppressing compressor blade oscillations. Nonlinear Dyn. 2017;90:1727-53.
- [50] Hamed YS, Kandil A, Machado JT. Utilizing macro fiber composite to control rotating blade vibrations. Symmetry. 2020;12:1-23.
- Hamed YS, Kandil A. Integral resonant controller for suppressing car's oscillations and eliminating its inherent jump phenomenon. Eur J Pure Appl Math. 2023;16(4):2729-50.

14 — Hany Samih Bauomy

- [52] Fang F, Xia G, Wang J. Nonlinear dynamic analysis of cantilevered piezoelectric energy harvesters under simultaneous parametric and external excitations. Acta Mech Sin. 2018;34(3):561–77.
- [53] Garg A, Dwivedy SK. Piezoelectric energy harvester under parametric excitation: a theoretical and experimental investigation.

 J Intell Mater Syst Struct. 2020;31(4):612–31.
- [54] Xia G, Fang F, Wang Q, Zhang M. Performance analysis of piezoelectric energy harvesters with a tip mass and nonlinearities of
- geometry and damping under parametric and external excitations. Arch Appl Mech. 2020;90(10):2297–318.
- [55] Meirovitch L. Fundamentals of vibrations. New York: Waveland Press; 2010.
- [56] Meesala VC, Hajj MR. Parameter sensitivity of cantilever beam with tip mass to parametric excitation. Nonlinear Dyn. 2019;95(4):3375–84.
- [57] Nayfeh AH. Perturbation methods. New York: John Wiley & Sons; 2008.